A CFD-Based Examination of Rotor-Rotor Separation Effects on Interactional Aerodynamics for eVTOL Aircraft

Richard Healy *
PhD Student

Matthew Misiorowski
PhD Graduate, 2019, Professor and MOVE Director

Farhan Gandhi
Redfern

Center for Mobility with Vertical Lift (MOVE), Rensselaer Polytechnic Institute, Troy, NY

This study systematically investigates the aerodynamic interactions of a two-rotor system with a front rotor and an aft rotor aligned with the direction of flow. The rotors are 5.5 ft diameter fixed-pitch rotors operating at approximately 12 lb/ft^2 disk loading, representative of large eVTOL aircraft. Fluid flow is simulated using the commercial Navier–Stokes solver, AcuSolve, with a detached eddy simulation (DES) model. Simulations were performed nominally at 40 kt edgewise flight for nine cases corresponding to three values of longitudinal hub–hub separation (2.5*R*, 3*R*, 3.5*R*) and three values of vertical offset (0, 0.25*R*, 0.5*R*). Aft rotor performance was compared to an isolated rotor operating in the same conditions in order to quantify the effects of rotor–rotor interaction. For the cases where the aft rotor is closest to the front rotor (2.5*R* longitudinal offset, zero vertical offset), the aft rotor produced 8.4% less thrust and required 13.4% higher torque than a rotor in isolation. When vertical rotor separation was increased, interactional aerodynamic effects decreased. For a 2.5*R* longitudinal offset, increasing the vertical offset to 0.5*R* decreased the lift deficit to 4.6% and the torque penalty to 6.8%. Increasing the longitudinal offset to 3.5*R* (while keeping the vertical offset at zero) also reduced interactional aerodynamic effects, but reductions in lift deficit and torque penalty were smaller than those observed with 0.5*R* vertical offset. Reducing disk loading was found to strengthen interactional aerodynamic effects, with an 11.5% thrust deficit at 6 lb/ft^2 compared to 9.0% at 12 lb/ft^2. An increase in flight speed also increased interactional aerodynamic penalties from 5.4% thrust deficit at 20 kt to 12.2% at 60 kt. The increased interactional aerodynamic penalties with the reduction in disk loading and increase in flight speed were both attributed to an increase in wake skew angle and the resulting decrease in separation between the aft rotor disk and front rotor wake.

Introduction

While hobbyists, recreational users, and enterprising videographers have been operating small multi-copters for a long time, the last few years have seen a tremendous interest in larger multirotor electric VTOL (eVTOL) aircraft for urban air mobility, commercial package delivery, cargo, and military/law-enforcement applications, among others. The current batteries powering most of these eVTOL aircraft exhibit very low-energy density relative to the hydrocarbon fuels used by larger conventional VTOL aircraft. With this limitation, it is especially important to maximize the aerodynamic performance of eVTOL aircraft in order to realize practical payload capacity, endurance, and range. Since these metrics were not as important to recreational users of smaller multi-copters, they have not previously received much consideration. One area that requires particular attention is the understanding of the interactional aerodynamic effects of multiple rotors operating in close proximity and their impact on aerodynamic performance.

A number of recent studies have used high-fidelity computational fluid dynamics (CFD) to simulate and understand the complex flows associated with interactional aerodynamics of rotors operating in close proximity. Yoon et al. (Refs. 1, 2) used CFD to investigate the effects of turbulence modeling and rotor separation on an XV-15 derivative quadcopter in hover and determined that decreasing the separation between rotors reduces the thrust generated by up to 4%. At the smaller scale, Yoon et al. simulated the DJI Phantom 3 and SUI Endurance quadcopters (Ref. 3) and determined that at 10 m/s cruise, the rear rotors produced up to 28% less thrust than if operating in isolation. Other work by Diaz and Yoon (Ref. 4) found that vertical rotor separation on a quadcopter via over/under mounting influenced rotor interaction in cruise.

Misiorowski et al. also used high-fidelity CFD to simulate quadcopters operating in cruise in the plus and cross configurations (Ref. 5) and provided physical insights into the difference in interactional aerodynamics for the two configurations. Notably, they reported that in the plus configuration, the side rotors operating in the upwash of the front rotor wake showed lift and power benefits. This phenomenon was recently corroborated by another study by Duivenvoorden et al. using computational and experimental methods (Ref. 6). Healy et al. examined the effects of rotor canting on multirotor interactional aerodynamic effects and also studied multirotor assemblies in ground effect (Refs. 7, 8). Over the last few years, NASA has developed a reconfigurable Multirotor

*Corresponding author; email: healyr@rpi.edu.

Revised version of paper presented at the 75th Annual Forum of the Vertical Flight Society, Philadelphia, PA, May 13–16, 2019. Manuscript received December 2020; accepted August 2021.

 © 2022 Vertical Flight Society

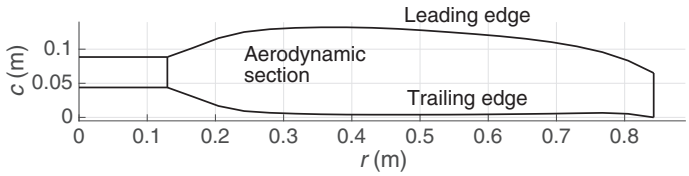

Fig. 1. Blade planform (chord distribution).

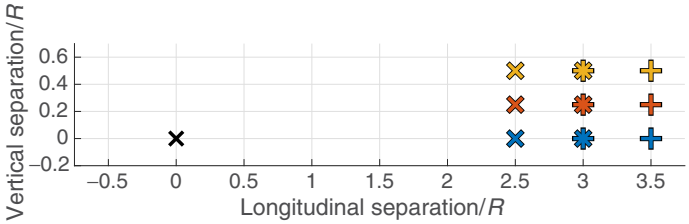

Fig. 3. Aft-rotor hub position relative to front rotor.

Testbed (MTB) where the relative positions and orientations of various rotors can be changed. Experiments conducted on this testbed by Russell and Conley (Ref. 9) have shown reductions in aft rotor thrust previously reported in computational studies. Researchers from NASA have also compared multirotor aerodynamic interaction effects using a midfidelity CFD analysis (Ref. 10) to the MTB test results.

Rather than focus on a specific multicopter configuration, the present study conducts high-fidelity CFD simulations of a unit comprising of two large (5.5 ft diameter) eVTOL rotors aligned in the direction of flight while parametrically varying the longitudinal and vertical spacing between the rotors. Further, variations in rotor disk loading and forward speed are also examined. As in Ref. 5, the simulations are conducted using the commercial Navier–Stokes solver, Acusolve (Ref. 11), and changes in interactional aerodynamic effects, with changes in the above parameters are examined and discussed.

Analysis

System definition

The rotor used in the current study is a modified $5\frac{1}{2}$ ft diameter two-bladed Whirlwind propeller (Ref. 12). The blade chord distribution is shown in Fig. 1. The original Whirlwind propeller is untwisted, fixed pitch and intended for axial flow applications. Most eVTOL designs utilize twisted fixed pitch rotors, so an appropriate root pitch value and twist are first selected for this study.

The Rensselaer Multirotor Analysis Code (RMAC) (Ref. 13), based on blade element theory (BET) with 3×4 finite state Peters–He inflow representation is used to evaluate the performance associated with possible modifications to the whirlwind propeller. For a sweep of tip pitch and twist rates, the rotor speed is trimmed in hover to match a preselected target disk loading representative of a large eVTOL aircraft (12 lb/ft^2 (Ref. 14)). Figure 2 shows the corresponding tip Mach number for the trimmed rotor speed at each tip pitch and twist rate, and the associated power requirement. A tip pitch of 12° and twist rate of $-12°/R$ is found to be a good balance between low tip Mach number ($M = 0.56$) and low power. To maintain a hover disk loading of 12 lb/ft^2, a blade rotational speed of 2170 RPM is required.

CFD simulations are conducted at a forward speed of 40 kt, with the majority of the simulations being for a two-rotor unit comprising of a clockwise-spinning front rotor and a counterclockwise-spinning aft rotor set at various separation distances relative to the front rotor, as shown in Fig. 3. The two-rotor unit is set at a nose-level pitch attitude relative to the freestream as many large eVTOL designs utilize a dedicated propeller for forward propulsion. The aft rotor of the two rotor unit is set at 2.5, 3, and 3.5 rotor radii longitudinal separation (hub to hub) from the front rotor, in the freestream direction. Simulations include the aft rotor in-plane, as well as at vertical offsets of 0.25 and 0.5 rotor radii above the front rotor. All of the simulated two-rotor configuration cases are shown in Fig. 3 (nine cases in all).

Computational method

CFD simulations are conducted using the commercial Navier–Stokes solver AcuSolve, which uses a stabilized second-order upwind finite element method and has been validated for external aerodynamic flows (Refs. 15, 16). AcuSolve simulation results for an SUI Endurance rotor in hover were previously shown to compare well against experiment in Ref. 5 where thrust at two different rotor speeds in hover matched experiment within 3%. AcuSolve has also been used for other rotorcraft simulations in Refs. 5, 7, 8, 17, and 18.

For a two-rotor unit, the computational domain is shown in Fig. 4, comprising of a rectangular prism with far-field boundary conditions on the front and top surfaces set to the freestream velocity. The sides, bottom, and rear of the computational domain are set to outflow with backflow conditions enabled, which allows for flow in either direction across the boundary with zero pressure offset. All boundaries of the computational domain are at least 25 rotor radii away from the center of the two rotor unit in all directions. As indicated in Fig. 4, the computational domain consists of two rotating volumes (one for each rotor) where the mesh inside the volume rotates along with the rotor blades. Each rotating volume is a

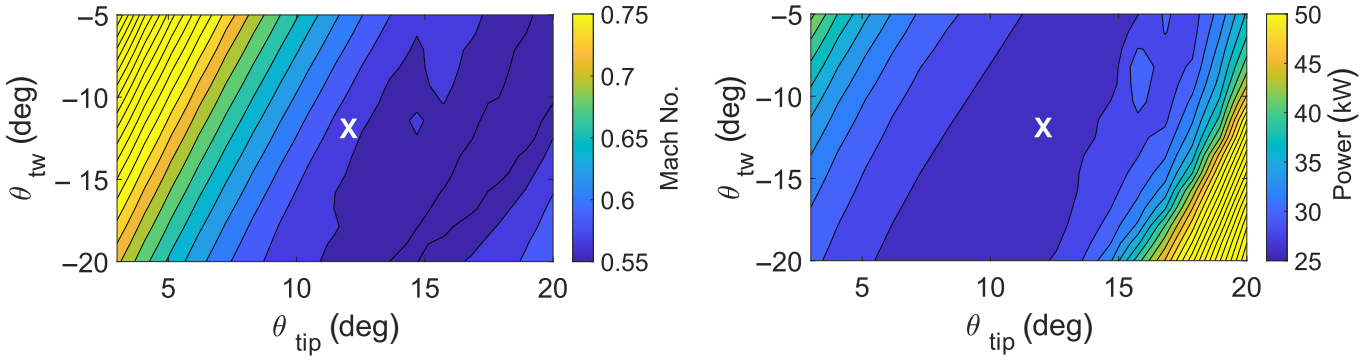

Fig. 2. Tip Mach number and power requirement for variation in twist rate and pitch setting. Selected twist rate and pitch marked with "X".

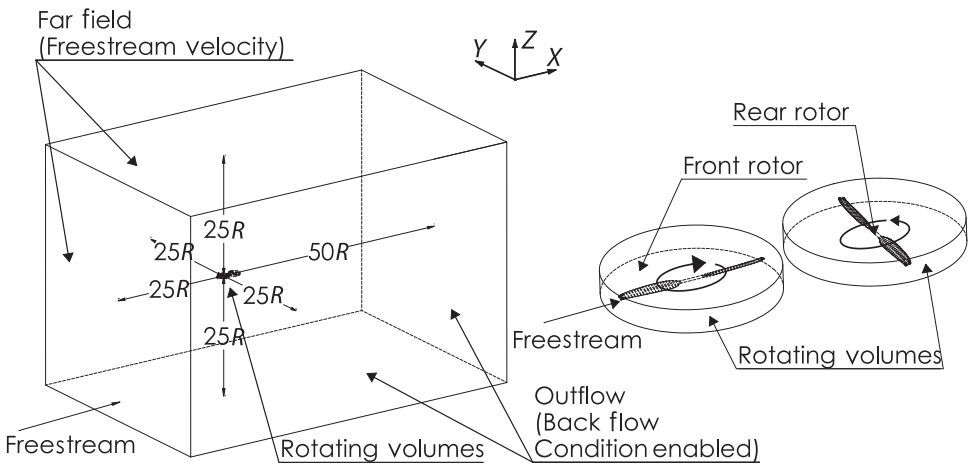

Fig. 4. Diagram of the computational domain.

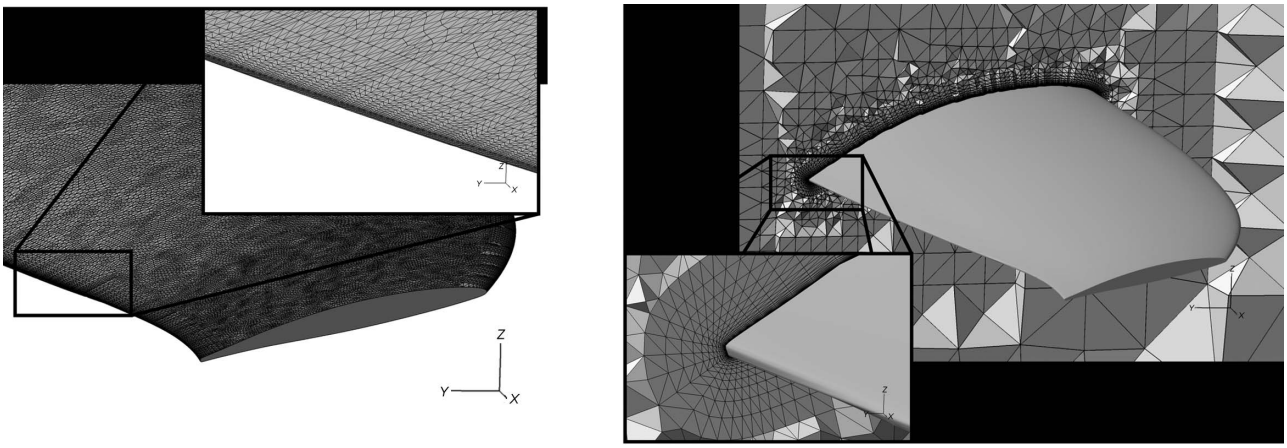

(a) Blade surface mesh near blade tip **(b) Chordwise slice through the mesh**

Fig. 5. Mesh visualization.

cylinder with radius 1.06 rotor radii. The height of the cylinder extends two tip chord lengths above and below the rotor plane. Each rotating volume is bounded by a sliding mesh interface which passes information to and from the nonrotating volume that comprises the remainder of the computational domain.

The domain was discretized using a mesh comprised entirely of unstructured tetrahedral elements. Within both rotating volumes, the blade surface mesh was set to ensure 200 elements around the airfoil contour. The elements on the blade were refined by a factor of 10× near the leading (0–10% chord) and trailing edge (90–100% chord), compared to the elements along the remainder of the chord. A portion of the blade surface mesh is shown in Fig. 5(a). The boundary layer in the wall normal direction is highly resolved, with the first element height set to ensure $y+ < 1$, and comprising 25 layers. A cross-sectional slice through the mesh in Fig. 5(b) shows the boundary layer elements around the airfoil. The results of a mesh refinement study for an isolated Whirlwind rotor are reported in the Appendix. These results were used to select the number of chordwise elements on the blade, leading and trailing-edge refinements, and the boundary layer refinement.

When simulating the two rotor system, a well-resolved wake region is needed to accurately predict the influence of one rotor's wake on another. With this in mind, a wake refinement zone is established for the off-body

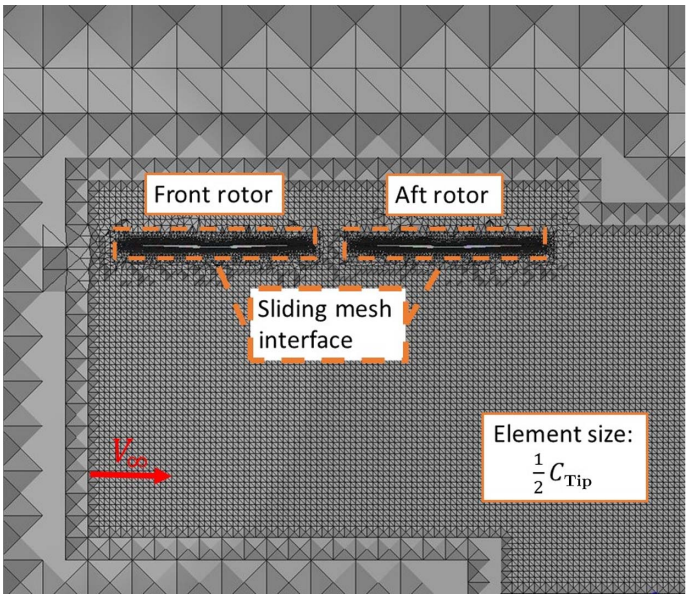

Fig. 6. Cross section of wake mesh refinement.

Table 1. Average rotor thrust and torque for aft rotors simulated with different wake refinement element sizes

Wake Element Size	Thrust (N)	Thrust Difference to $C_{tip}/4$	Torque (Nm)	Torque Difference to $C_{tip}/4$
$C_{tip}/1$	1203	3.7%	127	1.4%
$C_{tip}/2$	1232	1.4%	125.2	0.001%
$C_{tip}/4$	1249	–	125.3	–

area around the rotors, both inside the rotating volumes, as well as in the surrounding nonrotating volume. This region extends $0.6R$ above the rotor plane and $3R$ below (Fig. 6). Downwind of the rotors, the wake refinement zone is skewed downwards to better capture the rotor wakes as they convect downstream. In order to better understand the impact that additional degrees of wake refinement have on the solution, another mesh refinement study was performed, this time varying the wake refinement element size. Here, the impact of wake refinement on interactional aerodynamic prediction is of interest, so this study was performed on a two-rotor system in 40 kt edgewise flight with $2.5R$ longitudinal hub–hub separation and no vertical spacing. Three element sizes in the wake refinement region were considered: $C_{tip}/1$, $C_{tip}/2$, and $C_{tip}/4$ (where C_{tip} is the blade tip chord), which correspond to computational domains comprising 75, 125, and 367 million elements, respectively. Table 1 reports thrust and torque produced by the aft rotor for each refinement increment. The thrust and torque for a wake refinement size of $C_{tip}/2$ is found to differ from that with a size of $C_{tip}/4$ by less than 1.5%. Considering the substantial computational cost associated with further refinement of the wake, $C_{tip}/2$ is chosen as an acceptable wake refinement element size for this study. Using this degree of wake refinement, the entire computational domain is comprised of 125 million elements, with 33 million in each rotating volume, and 59 million in the nonrotating volume.

A DES is used with the Spalart–Allmaras (SA) turbulence model for all cases. All simulations were run initially using time steps corresponding to 10° of rotation for several revolutions to reduce computational cost of the rotor wake development. Each simulation was then restarted for additional revolutions at 1° time steps until convergence was achieved. The initial 10° time steps are possible without causing numerical divergence due to the stability afforded by the streamline upwind Petrov–Galerkin stabilized finite element method and generalized-α implicit time integration method. The latter method was designed to suppress high-frequency disturbances and allow solution stability with Courant–Friedrichs–Lewy number greater than 1 (Refs. 19, 20). All runs were performed on 512 2.6 GHz Intel Xeon E5-2650 processors, part of the Center for Computational Innovations at Rensselaer Polytechnic Institute. With an average simulation wall time of 146 h (6 days) for each case, the total cost for simulations presented in this study exceeds 2000 h (90 days) of wall time.

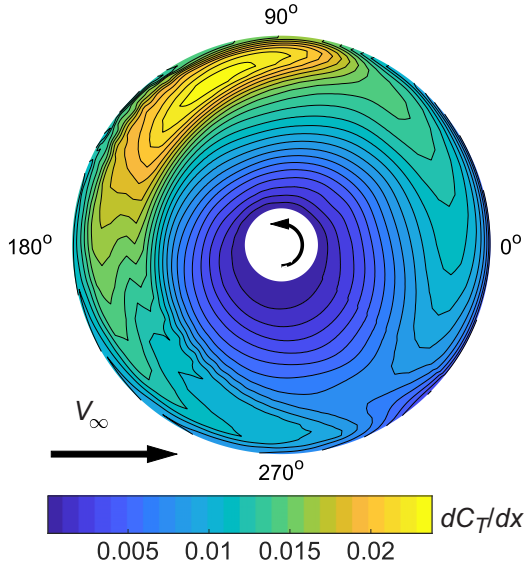

Fig. 7. Sectional thrust coefficient, dCt/dx, for isolated rotor.

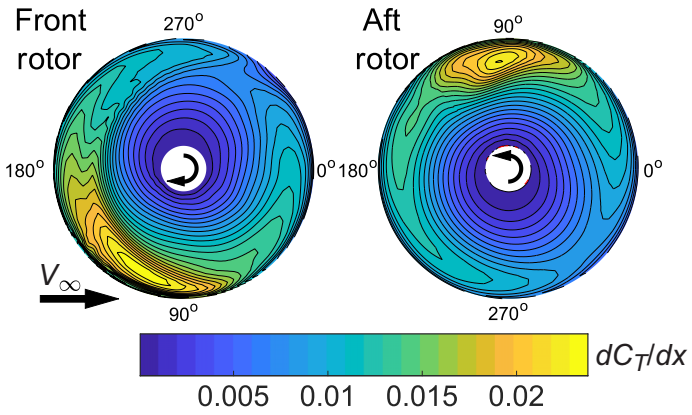

Fig. 8. Sectional thrust coefficient, dCt/dx, for 2.5 rotor radii separation.

Results

Isolated rotor aerodynamics

Forward flight simulations were conducted to first evaluate and analyze thrust production of an isolated rotor. Figure 7 shows the sectional thrust coefficient (dC_T/dx) for a counterclockwise spinning isolated rotor in 40 kt edgewise flow at 2170 RPM. This represents the operational state of the aft rotor in the system described above without the presence of a front rotor. A region of higher thrust can be seen on the advancing side of the rotor between $\psi = 100$–135°. This feature is consistent with that seen in Ref. 5 and is caused by higher dynamic pressure on the advancing side of the rotor, along with the longitudinal inflow variation (Ref. 21).

Interactional aerodynamics in a two rotor system

With the thrust properties of an isolated rotor established, the thrust production of a two-rotor system is investigated. Figure 8 shows the sectional thrust coefficient (dC_T/dx) for a two-rotor system with $2.5R$ longitudinal separation and no vertical separation. Compared to the isolated counterclockwise spinning rotor (Fig. 7), the aft rotor of this configuration exhibits a much smaller area of high-thrust centered around $\psi = 90^\circ$. The front rotor (also set at zero pitch attitude and spinning at 2170 RPM) exhibits no notable difference from an isolated clockwise rotor, indicating the presence of the aft rotor has no notable effect on the front rotor.

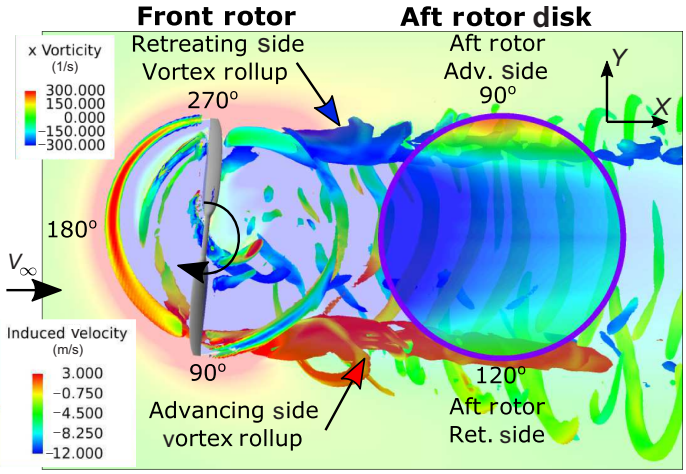

Fig. 9. Q-Criterion (20,000) of isolated rotor wake colored by vorticity in the freestream direction and induced velocity in the region of the aft rotor disk.

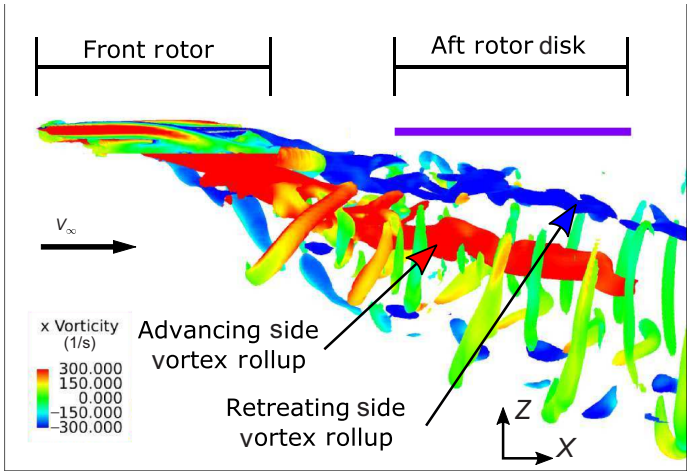

Fig. 10. Q-Criterion (15,000) of isolated rotor wake colored by vorticity in the freestream direction.

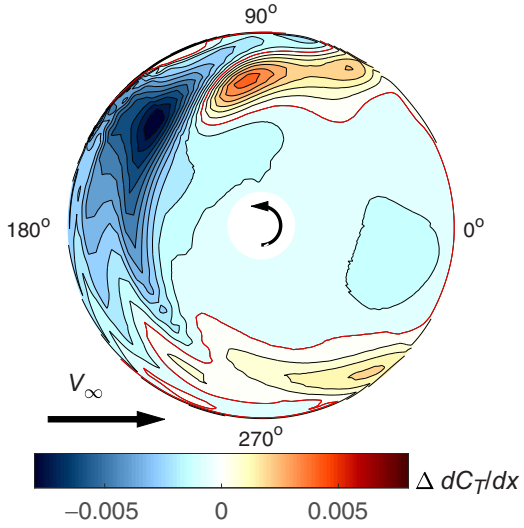

Fig. 11. Sectional thrust coefficient difference, $\Delta dC_T/dx$ (2.5R longitudinal separation subtracting isolated).

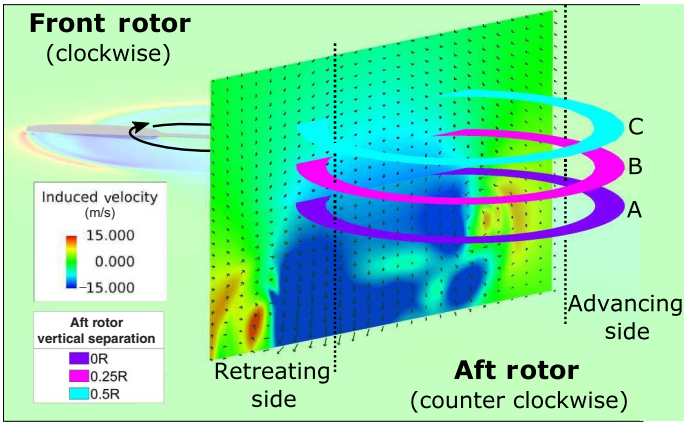

Fig. 12. Velocity induced by the front rotor on the area occupied by the aft rotor at 2.5*R* longitudinal separation.

Front rotor wake aerodynamics

The aerodynamics of a front rotor in isolation is investigated in order to gain insight on how the front rotor interacts with the aft rotor. Figure 9 shows the Q-criterion for an isolated rotor colored by X-vorticity. The region occupied by an aft rotor with 2.5*R* longitudinal separation and no vertical separation is also shown, colored by *Z*-induced velocity. Inside the wake, the vortex rollup from both the front rotor's advancing and retreating sides induces downwash, indicated by the blue region on the location of the aft rotor disk (no aft rotor actually present in the simulation). Downwash is stronger on the front of the rotor disk and grows progressively weaker towards the back of the rotor disk as the front rotor wake convects downwards. However, outside the wake, the vortex rollup induces upwash. The wake from the front rotor is observed to tilt toward its advancing side as it convects downstream. As a result, the retreating side of the aft rotor sees only downwash, but the advancing side of the aft rotor (which lies outside the front rotor wake) sees front rotor wake induced upwash.

Figure 10 shows the Q-criterion for an isolated clockwise spinning rotor, colored by X-vorticity as viewed from the side. The Biot–Savart law suggests that both the strength and proximity of the vortex rollup relative to the aft rotor disk will influence their induced downwash. While the advancing side vortex rollup in red is stronger (due to greater thrust production on the advancing side), it convects faster downward than that the blue retreating side vortex rollup due to the higher lift generation and higher downwash on the front rotor's advancing side. By the time the wake reaches the aft rotor disk, the advancing side rollup vortex, albeit stronger, has convected further downward than the retreating side rollup vortex. The increased distance between the advancing side vortex rollup and the aft rotor results in less downwash induced on the retreating side of the disk (as seen in Fig. 9), despite the relatively greater vortex strength.

The presence of downwash and upwash on the aft rotor disk discussed above are partly what cause the change in its rotor thrust relative to an isolated rotor operating at the same conditions (forward speed, pitch attitude, and RPM). Figure 11 shows the difference in the sectional thrust coefficient between an isolated aft rotor and an aft rotor with 2.5*R* longitudinal separation. Downwash seen in Fig. 9 causes a decrease in thrust near the front of the rotor. Additional downwash on a blade element reduces the effective angle of attack by increasing the local inflow angle. The reduction in angle of attack on the blade element reduces local blade

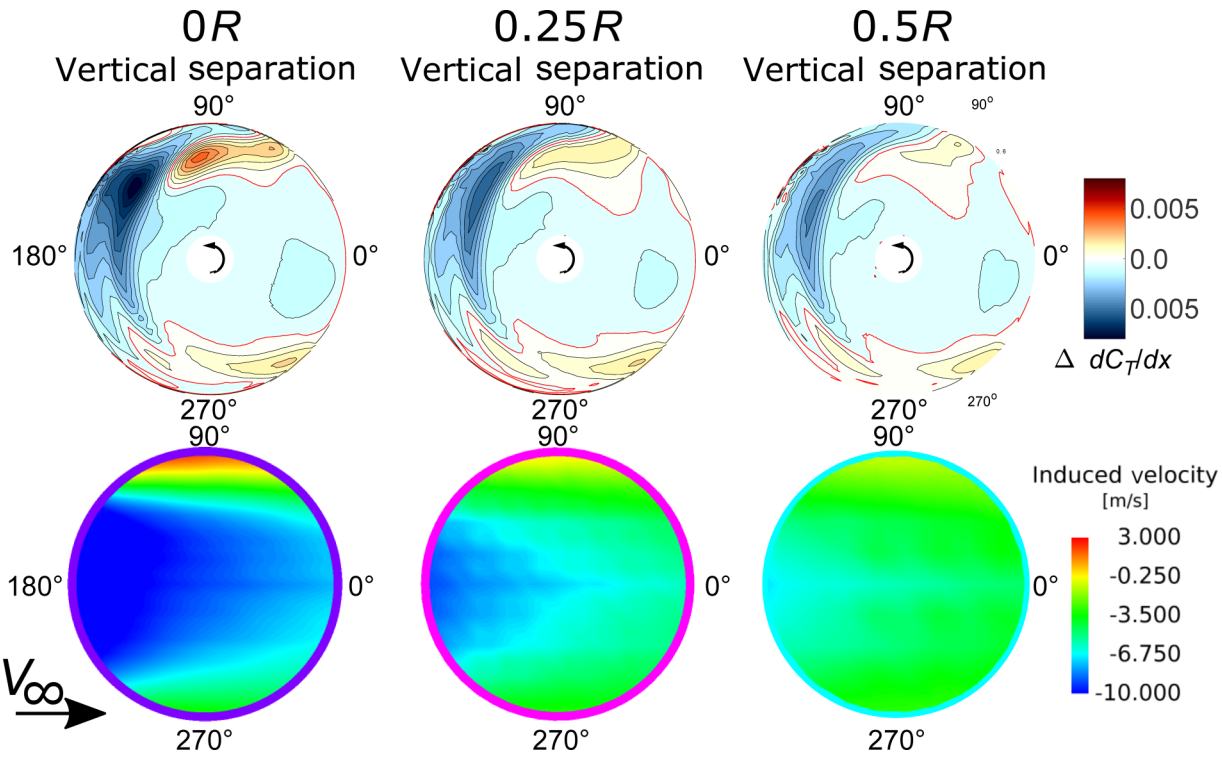

Fig. 13. Difference in the sectional thrust coefficient and induced velocity experienced from the front rotor for aft rotors with different vertical separations and 2.5*R* longitudinal separation.

lift. While the presence of the aft rotor may influence the distribution of front rotor induced downwash, this effect is thought to be small. Outside of the front rotor wake, upwash is induced from either the advancing or retreating side vortex rollup. A region of increased thrust is seen outboard on the advancing side due to upwash from the front rotor's retreating side vortex rollup.

The difference in rotor thrust observed between an aft rotor in a two rotor system and an isolated rotor is similar to that seen in Ref. 5. In both cases, the aft rotor experiences a loss in lift on the front of the rotor disk. Additionally, a region of increased thrust is seen at about $\psi = 90^\circ$ due to upwash from the front rotor's retreating side vortex rollup.

Impact of rotor spacing on thrust

The velocity induced by the front rotor on the aft rotor disk depends on the relative position of the aft rotor disk (Fig. 3). Figure 12 shows the velocity induced by an isolated front rotor over a vertical plane cutting through the front of the aft rotor disk situated at 2.5*R* longitudinal separation and three different vertical positions. The vertical slice is positioned 2/3*R* upstream of the aft rotor center. A region of blue downwash can be seen over this vertical plane cutting through the forward section of the aft rotor locations (no aft rotor actually present in this simulation). As the aft rotor is moved up from position A (in plane with the front rotor) to positions B and C (0.25*R* and 0.5*R* vertical offset, respectively), the downwash in the rotor plane decreases. The figure also shows the position of the front rotor's advancing and retreating side tip vortices. The retreating side tip vortex, which generates upwash and lift increment on the aft rotor's advancing side (Figs. 9 and 11), is further from the aft rotor as it moves up to positions B and C. Thus, the advancing side upwash and lift increment can be expected to weaken.

Figure 13 shows the difference in sectional thrust coefficient (thrust coefficient of aft rotor minus that of an isolated rotor at the same operating conditions) for aft rotors located at 2.5*R* longitudinal separation and different vertical separations. The velocity induced by an isolated front rotor at the corresponding location occupied by each aft rotor is also presented. As the aft rotor is moved up, out of the plane of the front rotor, the interactional aerodynamic effects are observed to diminish. Both downwash over the front section of the aft rotor disk and upwash on the outboard sections of the advancing blade decrease in magnitude. At 0.25*R* vertical separation, the peak loss in lift reduces in magnitude when compared to no vertical separation. Similarly, the peak increase in lift seen on the aft rotor's advancing side is also lower at 0.25*R* vertical separation. At 0.5*R* vertical, the magnitude of reduced lift is even smaller than that seen at 0.25*R* vertical separation. However, the change in peak lift reduction between 0*R* and 0.25*R* is greater than that seen between 0.25*R* and 0.5*R*. The increase in lift observed from vortex rollup on the aft rotor's advancing side also reduced as the aft rotor is moved up, away from the front rotor's retreating side vortex.

Figure 14 shows the difference in the sectional thrust coefficient (thrust coefficient of aft rotor minus that of an isolated rotor at the same operating conditions), at different longitudinal separations, and no vertical separation. Again, the induced velocity from the front rotor at the location occupied by each aft rotor is also shown. As longitudinal spacing increases, the decrease in thrust observed on the front of the rotor disk reduces in magnitude. Additionally, the increase in thrust seen on the advancing side of the aft rotor decreases in magnitude as well.

Figure 15 shows the relative difference in total rotor thrust between an aft rotor for the separation cases considered and an isolated rotor. An aft rotor with small longitudinal spacing and no vertical spacing (2.5*R*; 0*R*) experiences the largest loss in lift when in the presence of a front rotor (−8.4%). Keeping longitudinal spacing constant, as vertical spacing is increased, the aft rotor lift deficit reduces. At close longitudinal separation (2.5*R*), the change observed when moving from no vertical offset (8.4% lift deficit) to 0.25*R* (5.6% lift deficit) is greater than that

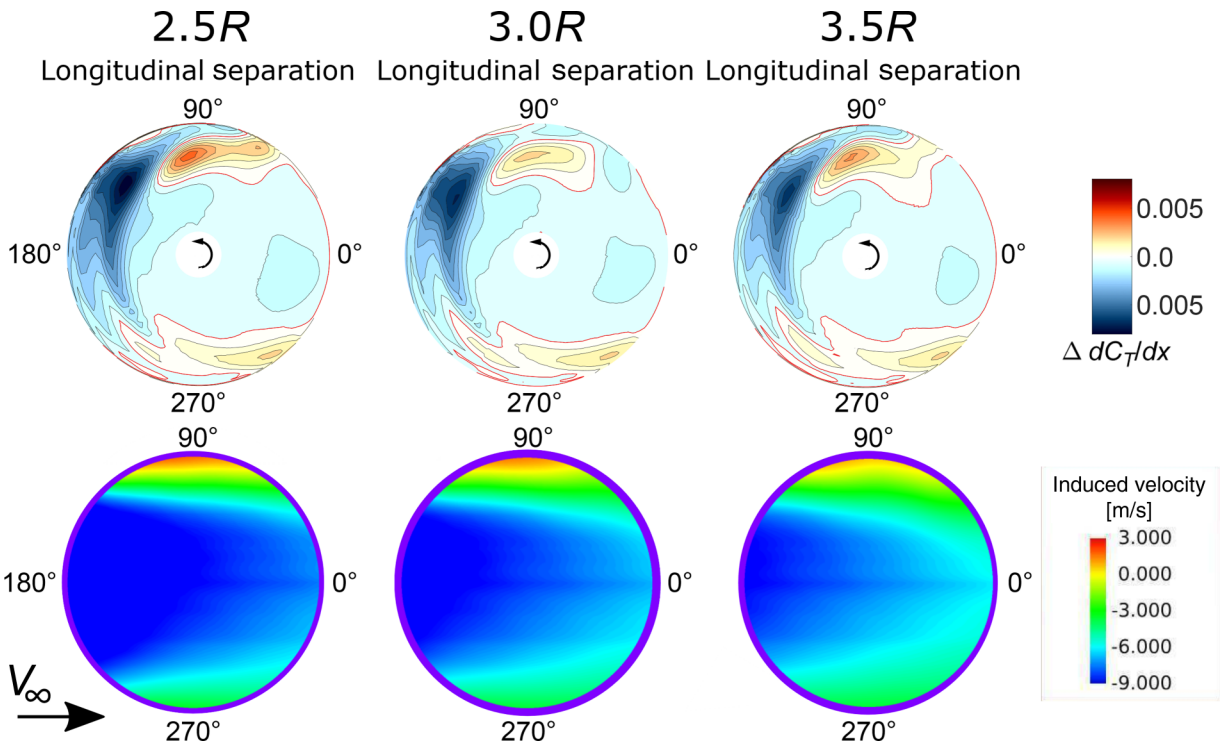

Fig. 14. Difference in the sectional thrust coefficient for aft rotors with different longitudinal separations and no vertical separation.

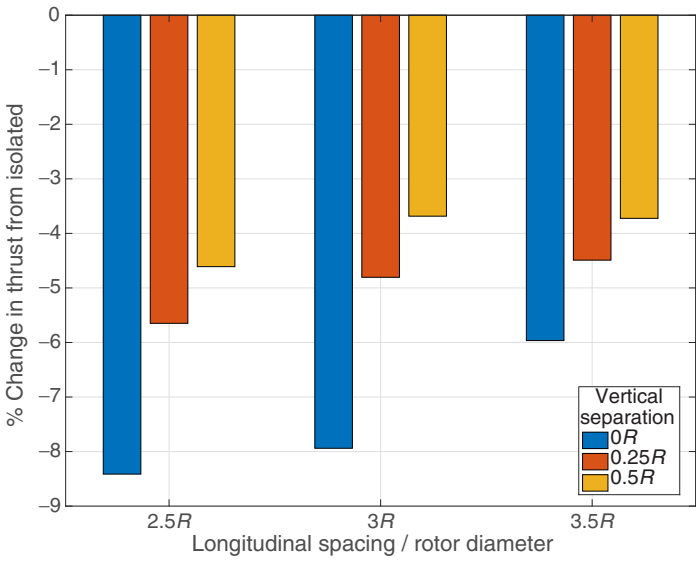

Fig. 15. Relative difference in rotor thrust for isolated and aft rotors in a two-rotor system at different longitudinal and vertical separations.

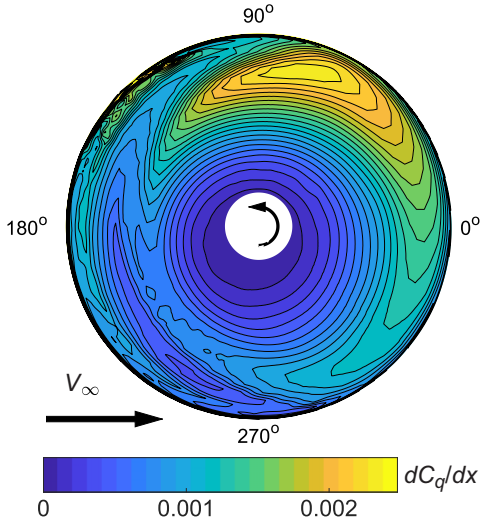

Fig. 16. Sectional torque coefficient dC_Q/dx for isolated rotor.

seen when moving from 0.25R to 0.5R (4.6% lift deficit). This trend holds for all longitudinal separations, where the biggest improvement is gained with the initial induction of vertical offset, and subsequent offsets provide smaller improvement.

Increasing longitudinal separation also reduces the negative impact of a front rotor. Keeping the aft rotor in-plane with the front rotor, an increase from 2.5R (8.4% lift deficit) to 3R (7.9% lift deficit) longitudinal spacing results in a smaller change than moving from 3R to 3.5R (5.8% lift deficit). However, this trend does not hold when considering higher vertical separations. If 0.25R vertical offset is used, an increase from 2.5R (5.6% lift deficit) to 3R (4.8% lift deficit) results in a larger change than from 3R to 3.5R (−4.3%). In general, these results suggest that both longitudinal separation and vertical separation are viable methods for reducing the rotor–rotor interaction in a two-rotor system; but a smaller 0.5R vertical offset is comparable to a 1R increase in longitudinal offset (without any vertical offset). If a vertical offset is already used, additional reductions in lift deficit due to increases in longitudinal separation are found to be small.

Impact of rotor spacing on torque

Figure 16 shows the sectional torque coefficient for an isolated rotor with 2.5R longitudinal separation and no vertical separation. Figure 17

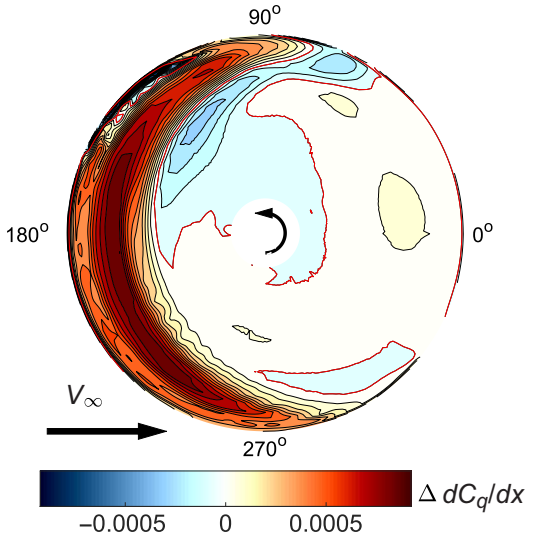

Fig. 17. Difference in the sectional torque coefficient, $\Delta dC_Q/dx$ (aft rotor minus isolated rotor) for 2.5R longitudinal separation and no vertical separation.

shows the difference in the sectional torque coefficient between an isolated aft rotor and an aft rotor with 2.5R longitudinal separation. The aft rotor exhibits more drag near the front of the rotor disk due to the high downwash induced by the front rotor in this area. Downwash on a blade element increases the local inflow angle, tilting the lift vector backwards, increasing induced drag.

Figure 18 shows the difference in the sectional torque coefficient (aft rotor minus isolated rotor) for aft rotors with 2.5R longitudinal separation and different vertical separations. As vertical separation is increased, the magnitude of high induced drag on the front of the rotor disk reduces. The less intense downwash experienced by the rotors with greater vertical separation leads peak drag to be lower in magnitude.

Figure 19 shows the sectional difference in the torque coefficient (aft rotor minus isolated) for aft rotors with various longitudinal separations and no vertical separation. As longitudinal separation is increased, the magnitude of drag on the front of the aft rotor disk slightly decreases. As with rotor thrust, the decreased downwash experienced by aft rotors with larger longitudinal spacing reduces interactional aerodynamic effects.

Figure 20 shows the net difference in rotor torque between aft rotors in a two-rotor system and an isolated rotor. The aft rotor with 2.5R longitudinal separation and no vertical separation exhibits the greatest increase in rotor torque (13.4%). As vertical separation is increased, the torque penalty reduces. At close longitudinal separation (2.5R), the improvement when going from no vertical offset (13.4% penalty) to 0.25R (9.8% penalty) is similar to that observed when progressing from 0.25R to 0.5R (6.8% penalty).

Longitudinal separation is also seen to influence aft rotor torque. When in-plane, relatively little change is seen when going from 2.5R (13.4% penalty) to 3R (12.9% penalty). However, moving from 3R to 3.5R (10.4% penalty) is seen to provide relatively more substantial improvement. At the highest vertical offset, increasing the longitudinal offset is relatively uninfluential (compare the three yellow bars on Fig. 20 for torque). Similar observation could also be made for thrust (Fig. 15).

Impact of rotor spacing on pitching moment

As observed in Fig. 7, the fixed pitch rotors simulated exhibit longitudinal thrust variation, which leads to strong nose-up pitching moment generation. However, as seen in Fig. 8, the peak thrust on the aft rotor tends to be located further back on the disk since lift loss in the presence of a front rotor is strongest at the front of the aft rotor. Thus, the nose-up pitching moment reduces (or in other words, experiences a nose-down moment relative to a rotor in isolation). When rotor spacing changes, so too does the longitudinal thrust variation and nose-up pitching moment. Figure 21 presents the aft rotor pitching moment difference (aft rotor pitching moment minus isolated) at each of the nine locations considered. Like with thrust deficit, increasing vertical and longitudinal separation reduces the relative nose-down pitching moment experienced. At the closest longitudinal spacing (2.5R), vertical separation has a minimal effect on pitch moment reduction. However, at further longitudinal spacing (3R and 3.5R), vertical separation weakens the relative nose-down pitching moment. In the longitudinal direction, increasing spacing is shown to lessen pitching moment reduction regardless of vertical spacing.

Influence of disk loading on interactional aerodynamics

The position of the front rotor wake in relation to the aft rotor has been seen to have a strong influence on the interactional aerodynamics at a fixed operating condition. However, changes in disk loading will modify the wake skew angle and hence the relative positioning of the front rotor wake relative to the aft rotor. In order to quantify the effects of disk loading on interactional aerodynamics, a two-rotor system with 3R longitudinal separation, and no vertical spacing was compared

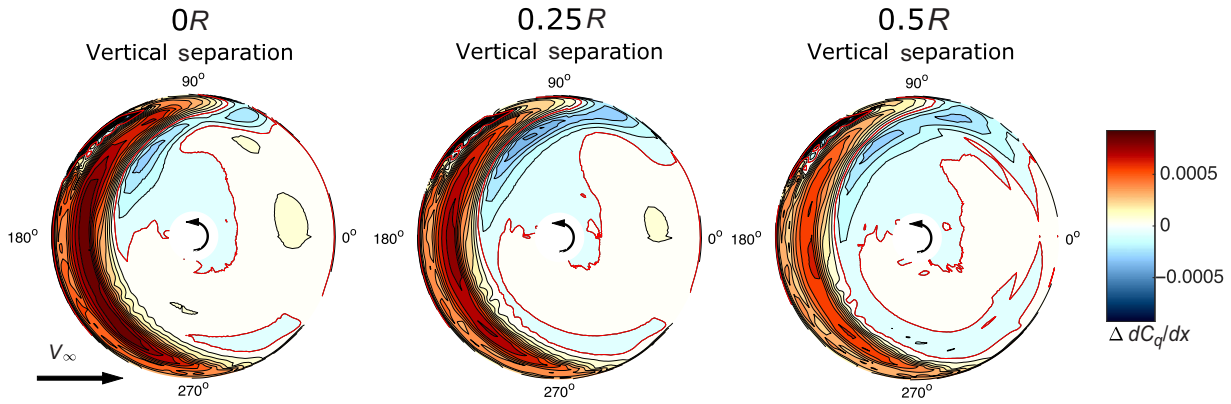

Fig. 18. Difference in the sectional torque coefficient, dC_Q/dr (aft rotor minus isolated rotor) for aft rotors with 2.5R longitudinal separation and different vertical separations.

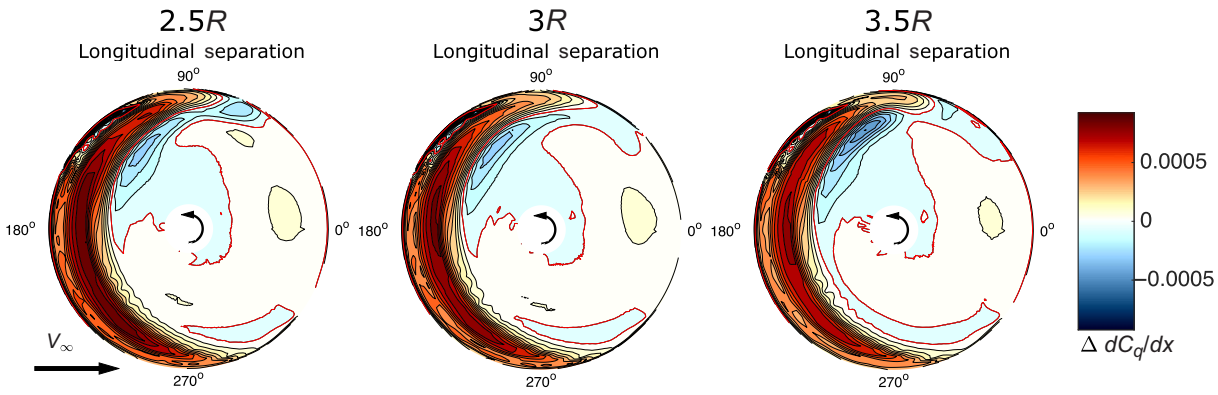

Fig. 19. Difference in the sectional torque coefficient, dC_Q/dx (aft rotor minus isolated rotor) for aft rotors with various longitudinal separation and no vertical separations.

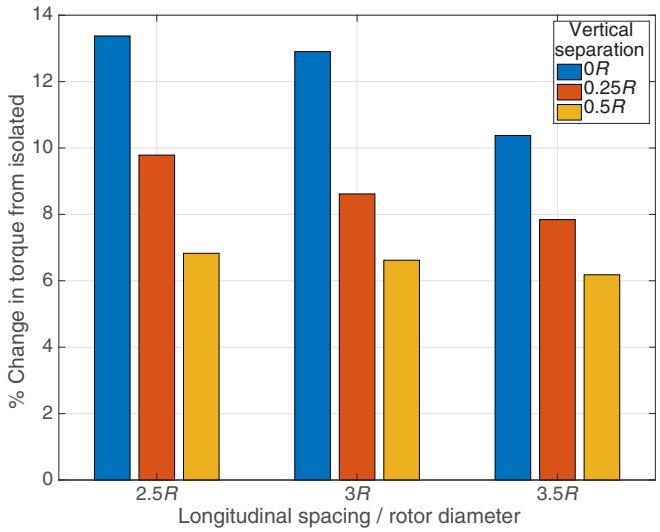

Fig. 20. Relative difference in torque for aft rotors in a two-rotor system.

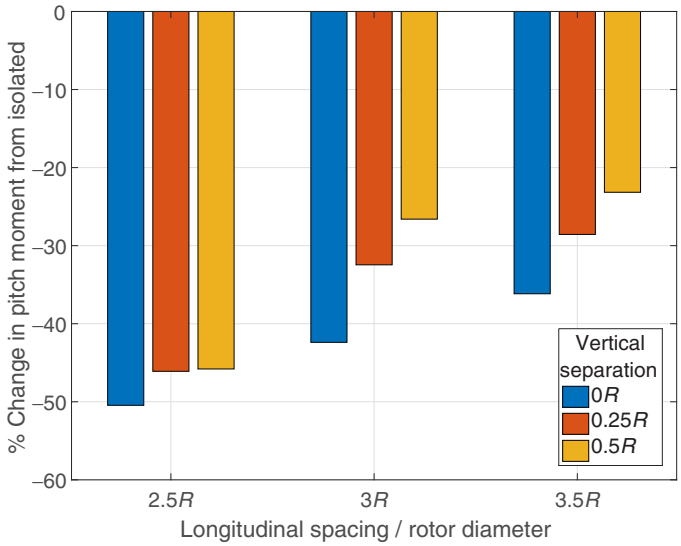

Fig. 21. Relative difference in pitching moment for aft rotors in a two-rotor system.

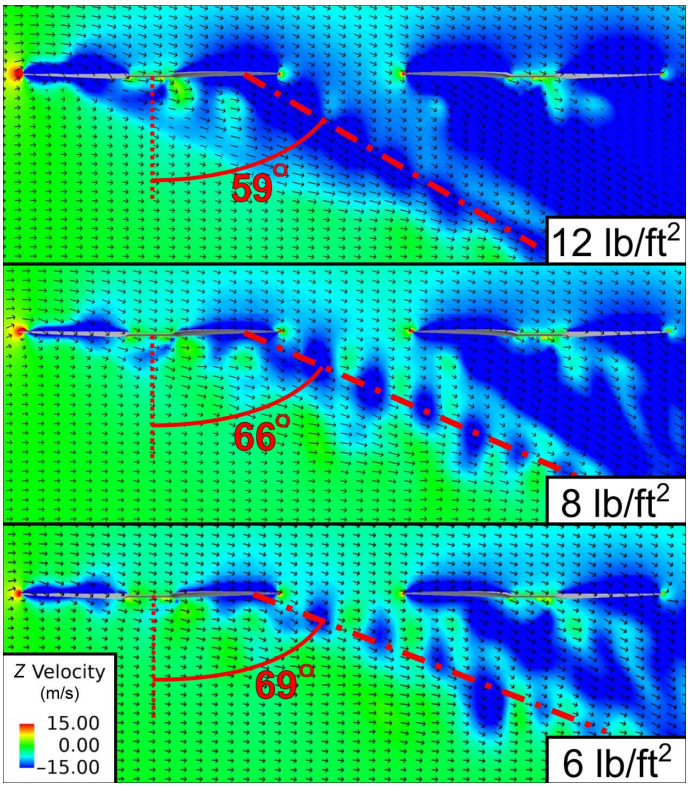

Fig. 22. Vertical velocity on a plane cutting through both rotor hubs as viewed from the left for multiple disk loadings.

at 40 kt and three disk loadings. In addition to the results already presented at 12 lb/ft^2, two additional simulations at 8 and 6 lb/ft^2 were performed. The disk loading was modified by changing the RPM of both rotors.

Figure 22 shows vertical velocity on a plane through both rotor hubs. Lines indicating the general direction of the front rotor wake are also presented as a qualitative means to compare the wake skew angle. As disk loading is reduced from 12 to 8 lb/ft^2, the front rotor's wake skew angle increases from approximately 59°–66°. When disk loading is further reduced to 6 lb/ft^2, the wake skew angle again increases to about 69°. As the wake skew angle increases, the position of the front rotor wake moves closer to the aft rotor disk. The reduced distance between wake and aft

Table 2. Aft rotor thrust change due to interactional aerodynamics at 40 kt and different disk loadings (aft rotor minus isolated rotor)

Disk Loading	12 lb/ft^2	8 lb/ft^2	6 lb/ft^2
Thrust difference	−9.0%	−10.0%	−11.5%

rotor disk leads to stronger downwash on the aft rotor and consequently an increase in thrust deficit.

Table 2 presents the change in thrust between the aft rotor and an isolated rotor in the same operating conditions for the three disk loadings. Thrust deficit was observed to reduce with disk loading, which is further supported by Refs. 5 and 2 who report 19–28% thrust difference at about 2 lb/ft^2. The aft rotor thrust deficit shows greater sensitivity at low disk loading, where the deficit is larger. Decreasing disk loading from 12 to 8 lb/ft^2 resulted in only an additional 1% reduction in aft rotor thrust. At lower disk loading values, smaller changes in disk loading (from 8 to 6 lb/ft^2) resulted in larger reductions (1.5%) in aft rotor thrust. Lower disk loading results in a larger wake skew angle. A larger wake skew angle positions the front rotor wake closer to the aft rotor disk, but the strength of the vorticity is expected to be lower than a higher disk loading case. Therefore, it would appear that the closer proximity of the front rotor wake to the aft rotor disk is more influential than the reduced vorticity strength when the disk loading decreases.

Influence of flight speed on interactional aerodynamics

Disk loading was found to have an influence on interactional aerodynamics by modifying the front rotor's wake skew angle. Another factor which is known to impact the wake skew angle is flight speed. In order to investigate the relationship between flight speed and interactional aerodynamic penalties, the 6 lb/ft^2 case was run at two additional flight speeds: 20 and 60 kt. Slices of vertical velocity as viewed from the left are shown for each flight speed in Fig. 23. Again, lines qualitatively representing the wake skew angle are also shown.

As flight speed increases, the freestream velocity convects the wake of the front rotor downstream faster, increasing the wake skew angle. As the wake skew angle increases, the wake of the front rotor moves closer to the aft rotor, and its influence on the aft rotor increases. With more downwash on the aft rotor, interactional aerodynamic penalties increase. At 20 kt, the wake of the front rotor has convected downward significantly by the time it reaches the aft rotor. At 40 and 60 kt, however, the wake of the front rotor is blown into the region occupied by the aft rotor. These differences become manifest in the interactional aerodynamic penalties presented in Table 3.

The aft rotor thrust deficit shows greater sensitivity at low cruise speed where the deficit is smaller. Increasing the speed from 20 to 40 kt resulted in an additional 6.1% reduction in aft rotor thrust. Further increasing the speed from 40 to 60 kt produced only an additional 0.7% reduction in aft rotor thrust. At low speeds (around 20 kt), the wake skew angle is small enough that the front rotor wake does not significantly influence the aft rotor. At around 40 kt, the front rotor wake skew is sufficiently large and its proximity to the aft rotor is sufficiently close to make it influential on the aft rotor aerodynamic performance. However, further increases in forward speed (and smaller increments in wake skew angle) appear to have marginal additional effect on the aft rotor aerodynamics.

Relation to Vehicle Design

Without the need for complicated mechanical drivetrains, distributed electric propulsion offers tremendous flexibility when it comes to rotor

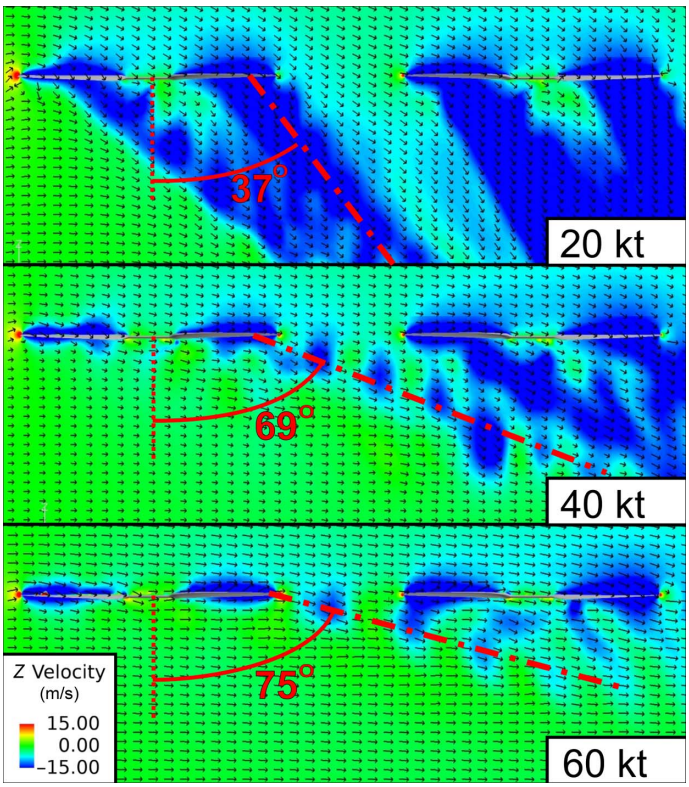

Fig. 23. Vertical velocity on a plane cutting through both rotor hubs as viewed from the left for multiple flight speeds.

Table 3. Aft rotor thrust change due to interactional aerodynamics at 6 lb/ft^2 disk loading and different flight speeds (aft rotor minus isolated rotor)

Flight Speed	20 kt	40 kt	60 kt
Thrust difference	−5.4%	−11.5%	−12.2%

placement. One aspect that should be considered when placing rotors on a vehicle is aerodynamic efficiency. If a part or all of a given vehicle's mission involves lifting rotor-borne forward flight, interactional aerodynamics between rotors will contribute to overall aerodynamic efficiency. While several factors contribute to interactional aerodynamic effects (wake skew angle, blade design, fuselage profile, etc.), the results of this work suggest it could be beneficial to increase spacing between rotors aligned with the freestream to minimize interactional penalties. Vertical separation (with the aft rotor set higher than the front rotor) is more effective than longitudinal separation if the rotor-mounting strategy permits such a choice. Reducing interactional aerodynamic penalties via rotor–rotor spacing could be especially important for more than two rotors in a track configuration. In this case, all rotors positioned behind the front rotor would be expected to produce a lift deficit due to the effects of the preceding rotor. Increasing longitudinal spacing, vertically offsetting the rotors in a stepped fashion, or both, could potentially improve aerodynamic performance. Based on the results of the disk loading and advance ratio studies, penalties are greater at larger wake skew angles (encountered at higher speeds and lower disk loadings). Thus, when interrotor separation cannot be increased due to footprint, sizing, or other design considerations, performance improvements may also be realized through modification of operating conditions. For example, for lift-compounded eVTOL, transitioning to rotor-borne flight (during ap-

Table 4. Average rotor thrust and torque for isolated rotors with different mesh parameters. The baseline mesh includes 12 boundary layer elements, 10× LE/TE refinement, and 200 elements around the airfoil contour

Mesh	Integrated Thrust (N)	Thrust % Difference from Baseline	Torque (Nm)	Torque % Difference from Baseline
Baseline	1174.1	–	74.8	–
4× Boundary layer elements	1172.2	0.16	74.6	0.27
2× LE/TE refinement	1175.8	0.14	75.1	0.4
2× Chordwise elements	1160.1	1.2	73.6	1.6

proach to landing) at as low a speed as possible may be beneficial as it reduces the wake skew angle and rotor–rotor aerodynamic interaction. Similarly, operating at high disk loading (which may be fairly typical of eVTOL vehicles) would minimize interactional aerodynamic penalties (although high disk loading, in and of itself is detrimental to hover and low-speed performance).

Conclusions

This study investigates the impact of longitudinal and vertical separation on the interactional aerodynamics of a counterrotating in-line two-rotor system in edgewise flight. Fluid flow simulations were performed using the commercial CFD code AcuSolve, with a DES. The rotating volume around each rotor interfaces with the remainder of the computational domain using a sliding mesh. All simulations were performed for twisted $5\frac{1}{2}$ ft diameter whirlwind propellers with 24° root pitch. Rotor RPM was set to nominally target 12 lb/ft^2 disk loading. In total, nine two-rotor system simulations were performed for varying longitudinal and vertical rotor separations at 12 lb/ft^2 disk loading and 40 kt cruise speed. In particular, three longitudinal hub-to-hub separations (2.5R, 3R, 3.5R), and three vertical separations (0R, 0.25R, 0.5R) were considered. Aft rotor thrust, torque, and pitching moment from each simulation were compared to those for an isolated rotor operating in the same conditions. Additional simulations were also performed for disk loading and cruise speed variations. Through these simulations, the following observations are made:

1) For all separation distances simulated, the wake of the front rotor induces downwash on the aft rotor disk. More downwash is observed on the front of the aft rotor disk than on the rear of the rotor disk due to downward front rotor wake convection with longitudinal distance. A lateral tilt of the front rotor wake towards its advancing side, as it convects downstream, results in the advancing tip of the aft rotor operating in the upwash of the front rotor's retreating side rollup vortex.

2) When compared to an isolated rotor in edgewise flight, the aft rotor of a two-rotor system is observed to produce less thrust and require greater torque, with the lift loss predominantly at the front of the rotor disk. In particular, an aft rotor 2.5R behind, and vertically aligned with the front rotor produces 8.4% less thrust than an isolated rotor, requires 13.4% higher torque, and shows a 50% reduction in nose-up pitching moment (compared to the case when no front rotor is present).

3) As vertical rotor spacing increases, and the distance between the aft rotor and the front rotor's wake grows larger, the downwash observed by the aft rotor reduces. The reduction in downwash causes lift deficit to reduce. Similarly, the torque penalty on the aft rotor decreases with vertical separation. For an aft rotor spaced 2.5R behind the front rotor, a 0.5R vertical offset reduces the lift deficit to 4.6%, and the torque penalty to 6.8%.

4) As longitudinal spacing increases, the downwash observed by the aft rotor again decreases. Increased longitudinal separation allows the front rotor wake to convect down farther by the time it reaches the aft rotor. The reduction in downwash causes the aft rotor lift deficit and torque penalty to decrease in magnitude. The improvements in lift and torque going from 2.5R to 3R longitudinal separation are modest, but larger improvements are seen going from 3R to 3.5R. A rotor at 3.5R longitudinal separation (and zero vertical offset) shows a 6.0% lift deficit, 10.4% torque penalty, and shows a 36% reduction in nose-up pitching moment (compared to an isolated rotor).

5) Over the range of parameters considered in this study, vertical separation was more effective in minimizing interactional aerodynamic effects. Compared to an aft rotor 2.5R behind the front rotor and with zero vertical offset exhibiting a lift deficit of 8.4%, increasing its vertical offset to 0.5R (same longitudinal separation of 2.5R) reduced the lift deficit to 4.6%. In contrast, increasing the longitudinal offset to 3.5R (keeping zero vertical separation) reduced the lift deficit to 6.0%. Similarly, compared to the 13.4% torque penalty for a rotor 2.5R aft and in-plane with the front rotor, increasing its vertical offset to 0.5R (same longitudinal position) decreases the torque penalty to 6.8%. In contrast, increasing the longitudinal offset to 3.5R (keeping zero vertical separation) decreases the torque penalty to 10.4%. With a 0.5R vertical offset of the aft rotor, a further increase in longitudinal offset (above 2.5R) produces limited benefits.

6) Variation in rotor disk loading and flight speed changed interactional aerodynamic effects on the aft rotor primarily through change in the front rotor wake skew angle and its effect on separation between the aft rotor disk and front rotor wake. Increases in the wake skew angle due to the reduction in disk loading or increase in flight speed are found to exacerbate interactional aerodynamic penalties. A relatively low disk loading of 6 lb/ft^2 is found to produce a relatively higher 11.5% thrust deficit (compared to 9.0% for 12 lb/ft^2). Similarly, increasing flight speed from 20 to 60 kt (while holding the disk loading at 6 lb/ft^2) was found to increase thrust deficit from 6% to 12%.

Appendix

Mesh refinement study

In order to ensure spacial convergence, a mesh refinement study was performed in which the surface mesh, leading edge/trailing edge refinement, and boundary layer were doubled independently for a 7° twisted whirlwind propeller. The results of the refinement study are shown in Table 4 and are used to ensure that predicted loads on an isolated rotor are not impacted by additional mesh refinement. For an isolated rotor in 40 kt edgewise flight, the thrust and torque changed by less than 1.5% and 2.0%, respectively, when compared to the baseline mesh (which is used for simulations in this study).

References

[1]Yoon, S., Pulliam, T. H., and Chaderjian, N. M., "Simulations of XV-15 Rotor Flows in Hover Using OVERFLOW," Proceedings of the AHS 5th Aeromechanics Specialists Conference, San Francisco, CA, January 22–24, 2014.

[2]Yoon, S., Lee, H. C., and Pulliam, T. H. "Computational Analysis of Multi-rotor Flows," Proceedings of the AIAA 54th Aerospace Sciences Meeting, San Diego, CA, January 4–8, 2016.

[3]Yoon, S., Diaz, P. V., Boyd, D. D., Jr., Chan, W. M., and Theodore, C. R., "Computational Aerodynamic Modeling of Small Quadcopter Vehicles," Proceedings of the 73rd Annual Forum of AHS International, Fort Worth, TX, May 9–11, 2017.

[4]Diaz, P. V., and Yoon, S., "High-Fidelity Computational Aerodynamics of Multi-rotor Unmanned Aerial Vehicles," Proceedings of the 2018 AIAA SciTech Forum, Kissimmee, FL, American Institute of Aeronautics and Astronautics, January 8–12, 2018.

[5]Misiorowski, M., Gandhi, F., and Oberai, A. A., "Computational study on rotor interactional effects for a quadcopter in edgewise flight," *AIAA Journal*, Vol. 57, no. 12, pp. 5309–5319, 2019.

[6]Duivenvoorden, R., Voskuijl, M., Morée, L., de Vries, J., and van der Veen, F., "Numerical and Experimental Investigation into the Aerodynamic Benefits of Rotorcraft Formation Flight," Proceedings of the 76th Annual Forum of the Vertical Flight Society, Virtual, October 5–8, 2020.

[7]Healy, R., Gandhi, F., Mistry, M., and Duffy, M., "A Computational Investigation of Multi-rotor Interactional Aerodynamics with Hub Lateral and Longitudinal Canting," Proceedings of the 76th Annual Forum, the Vertical Flight Society, Virtual, October 5–8, 2020.

[8]Healy, R., McCauley, J., Gandhi, F., and Sahni, O., "A Computational Investigation of Side-by-Side Rotors in Ground Effect," Proceedings of the 77th Annual Forum of the Vertical Flight Society, Virtual, May 10–14, 2021.

[9]Russell, C., and Conley, S., "The Multirotor Test Bed – A New NASA Test Capability for Advanced VTOL Rotorcraft Configurations," Proceedings of the 76th Annual Forum of the Vertical Flight Society, Virtual, October 5–8, 2020.

[10]Conley, S., Russell, C., Kallstrom, K., Koning, W., and Romander, E., "Comparing RotCFD Predictions of the Multirotor Test Bed with Experimental Results," Proceedings of the 76th Annual Forum of the Vertical Flight Society, Virtual, October 5–8, 2020.

[11]ACUSIM Software, Inc., "AcuSolve validation – NACA 0012 airfoil," Technical Report, http://altairhyperworks.com /ResourceLibrary.aspx?category=Case2010, 2010.

[12]Whirlwind Propellers, https://whirlwindpropellers.com/airboats /shop/razor-x/, 2018.

[13] Niemiec, R., and Gandhi, F., "Development and Validation of the Rensselaer Multicopter Analysis Code (RMAC): A Physics-Based Low-Fidelity Modeling Tool," Proceedings of the 75th Annual Forum of the Vertical Flight Society, Philadelphia, PA, May 13–16, 2019.

[14]Giannini, F., Kaufman, A., and Kearney, M., "Configuration Development and Subscale Flight Testing of an Urban Mobility eVTOL," Proceedings of the Aeromechanics Design for Transformative Vertical Flight of the AHS International, San Francisco, CA, January 16–18, 2018.

[15]ACUSIM Software, Inc., "Acusolve Validation – NACA 0012 Airfoil," Technical Report, https://www.altair.com/resource/acusolve-validation-naca0012-airfoil, 2010.

[16]Corson, D., Jaiman, R., and Shakib, F., "Industrial Application of RANS Modelling: Capabilities and Needs," *International Journal of Computational Fluid Dynamics*, Vol. 23, (4), 2009, 337–347.

[17]Misiorowski, M. P., Gandhi, F. S., and Oberai, A. A., "Computational Analysis and Flow Physics of a Ducted Rotor in Edgewise Flight," *Journal of the American Helicopter Society*, Vol. 64, October 2019, pp. 1–14.

[18]Misiorowski, M. P., Gandhi, F. S., and Oberai, A. A., "Computational Study of Diffuser Length on Ducted Rotor Performance in Edgewise Flight," *AIAA Journal*, Vol. 57, (2), 2019, pp. 796–808.

[19]Jansen, K., Whiting, C., and Hulbert, G., "A Generalized-Method for Integrating the Filtered Navier Stokes Equations with a Stabilized Finite Element Method," *Computer Methods in Applied Mechanics and Engineering*, Vol. 190, 2000, pp. 305–319.

[20]Brooks, A. N., and Hughes, T. J. R., "Streamline Upwind/Petrov–Galerkin Formulations for Convection Dominated Flows with Particular Emphasis on the Incompressible Navier–Stokes Equations," *Computer Methods in Applied Mechanics and Engineering*, Vol. 32, September 1982, pp. 199–259.

[21]Niemiec, R. and Gandhi, F., "Effects of Inflow Model on Simulated Aeromechanics of a Quadrotor Helicopter," Proceedings of the 72nd Annual Forum and Technology Display of the AHS International, West Palm Beach, FL, May 17–19, 2016.